



# Available online at www.sciencedirect.com

# **ScienceDirect**

Comput. Methods Appl. Mech. Engrg. 345 (2019) 1077-1093

Computer methods in applied mechanics and engineering

www.elsevier.com/locate/cma

# Global in time stability and accuracy of IMEX-FEM data assimilation schemes for Navier–Stokes equations

Adam Larios<sup>a</sup>, Leo G. Rebholz<sup>b</sup>,\*, Camille Zerfas<sup>b</sup>

Received 4 May 2018; received in revised form 8 August 2018; accepted 1 September 2018 Available online 15 September 2018

#### Abstract

We study numerical schemes for incompressible Navier–Stokes equations using IMEX temporal discretizations, finite element spatial discretizations, and equipped with continuous data assimilation (a technique recently developed by Azouani et al. (2014)). We analyze stability and accuracy of the proposed methods, and are able to prove well-posedness, long time stability, and long time accuracy estimates, under restrictions of the time step size and data assimilation parameter. We give results for several numerical tests that illustrate the theory, and show that, for good results, the choice of discretization parameter and element choices can be critical.

© 2018 Elsevier B.V. All rights reserved.

MSC classification: 35B42; 35Q30; 37L65; 65M12; 65M15; 65M70; 76B75; 93B52; 93C20

Keywords: Data assimilation; Navier-Stokes equations; Finite elements; Divergence-free finite elements

## 1. Introduction

Data assimilation (DA) refers to a wide class of schemes for incorporating observational data in simulations, in order to increase the accuracy of solutions and to obtain better estimates of initial conditions. It is the subject of a large body of work (see, e.g., [1–3], and the references therein). DA algorithms are widely used in weather modeling, climate science, and hydrological and environmental forecasting [2]. Classically, these techniques are based on linear quadratic estimation, also known as the Kalman Filter. The Kalman Filter, as well as variational methods such as 3D/4D Var, are described in detail in several textbooks, including [4,1–3], and the references therein.

Recently, a promising new approach to data assimilation was pioneered by Azouani, Olson, and Titi [5,6] (see also [7–9] for early ideas in this direction). This new approach, which we call AOT Data Assimilation, AOT-DA, or continuous data assimilation, adds a feedback control term at the partial differential equation (PDE) level that nudges the computed solution towards the reference solution corresponding to the observed data. A similar approach is taken by Blömker, Law, Stuart, and Zygalakis in [10] in the context of stochastic differential equations. While

E-mail addresses: alarios@unl.edu (A. Larios), rebholz@clemson.edu (L.G. Rebholz), czerfas@clemson.edu (C. Zerfas).

<sup>&</sup>lt;sup>a</sup> Department of Mathematics, University of Nebraska-Lincoln, Lincoln, NE 68588, United States

<sup>&</sup>lt;sup>b</sup> Department of Mathematical Sciences, Clemson University, Clemson, SC 29634, United States

<sup>\*</sup> Corresponding author.

the AOT-DA method looks somewhat similar to the so-called nudging or Newtonian relaxation methods introduced in [11,12], the specific use of interpolation in AOT-DA method is a crucial difference between the two methods, with major effects in terms of both implementation and convergence. For an overview of nudging methods, see, e.g., [13]. The AOT-DA algorithm is based on feedback control at the PDE level, described below. The first works on it assumed noise-free observations, but [14] adapted the method to the case of noisy data, and [15] adapted to the case in which measurements are obtained discretely in time and may be contaminated by systematic errors. Computational experiments on the AOT algorithm and its variants were carried out in the cases of the 2D Navier–Stokes equations [16], the 2D Bénard convection equations [17], and the 1D Kuramoto–Sivashinsky equations [18,19]. In [18], several nonlinear versions of this approach were proposed and studied. In addition to the results discussed here, a large amount of recent literature has built upon this idea; see, e.g., [20–32]. Although extensive research has been done on the theory of DA algorithms, there is currently little work on the numerical analysis of these algorithms, save [33], which studied a continuous-in-time Galerkin approximation of the algorithm, and [34] which studied a Galerkin in space, and explicit in time algorithm for the 2D Navier–Stokes equations (NSE).

In this paper, we propose and study discrete numerical algorithms of the NSE with an added data assimilation term and grad-div term, in 2D or 3D, and under the assumption that sufficiently regular solutions exist. In particular, we consider IMEX time stepping schemes and finite element spatial discretizations. We show that the particular element choice and/or stabilization parameters can make a dramatic difference in the success of the AOT-DA algorithm, and the time stepping algorithms also need careful consideration since time step restrictions can arise.

Briefly, the incompressible NSE are given by

$$u_t + (u \cdot \nabla)u - \nu \Delta u + \nabla p - \gamma \nabla(\nabla \cdot u) = f, \tag{1.1}$$

$$\nabla \cdot u = 0, \tag{1.2}$$

where u represents the velocity and p pressure. The viscosity is given by v > 0, and external forcing is f. Note that at the continuous level, the grad-div term is zero. The corresponding data assimilation algorithm is given by the system,

$$v_t + (v \cdot \nabla)v + \nabla q - v\Delta v + \mu I_H(v - u) - \gamma \nabla(\nabla \cdot v) = f, \tag{1.3}$$

$$\nabla \cdot v = 0, \tag{1.4}$$

where v is the approximate velocity and q the pressure of this approximate flow. The viscosity v > 0 and forcing f are the same as the above. The scalar  $\mu$  is known as the nudging parameter, and  $I_H$  is the interpolation operator, where H is the resolution of a coarse spatial mesh. The added data assimilation term forces (or nudges) the coarse spatial scales of the approximating solution v to the coarse spatial scales of the true solution v. The initial value of v is arbitrary.

We note that in all computational studies discussed above, the equations have been handled with fully explicit schemes (typically forward Euler). However, in explicit schemes, numerical instability is expected to arise from the term  $\mu I_H(v-u)$  on the right-hand side of (1.3) for large values of  $\mu$ , and thus an implicit treatment of this term has advantages. Thus, we study a BDF2 scheme for the data assimilation algorithm below. Fully implicit schemes can be costly though, due to the need to solve nonlinear systems, which can require, e.g., expensive Newton solves at every time step (Newton methods have other theoretical problems, discussed below). Therefore, we also study implicit–explicit (IMEX) schemes, which handle the nonlinear term semi-implicitly, but the linear terms (in particular,  $\mu I_H(v-u)$ ) implicitly.

In [35], it is argued (in the context of determining modes) that no higher-order Runge–Kutta-type methods or (fully) implicit methods of order greater than one can be constructed which satisfy the criteria of having the same discrete dynamics for u and v, and which use only the information of  $I_H(u)$  (as opposed to u) in the computation of v. This is the reason why we use backward-differentiation methods, although Adams–Bashforth/Adams–Moulton would also be suitable choices. We remark that, in the case of implicit methods, such methods do not make sense to use directly as one would need knowledge of the future; namely,  $I_H(u^{n+1})$ . However, by interpreting our simulations as being run "one time-step in the past", so that  $I_H(u^{n+1})$  is taken to be the most recent data, not future data that is unmeasured. The algorithms we propose in this work are consistent with the requirement stated in [35] that the right-hand side of the assimilated system not be evaluated more than once per time step. This is because the algorithms proposed here are only semi-implicit, and therefore do not require repeated solves due to the use of, e.g., Newton methods. We also note that typically multi-step methods require initializing the first few steps via another method, such as a higher-order Runge–Kutta method. However, we prove that for any initialization of the first few steps, the solutions generated by

the algorithm converge to the true solution. For example, the first few steps could all be initialized to zero. Thus, algorithms we present below have the advantage of needing no special scheme for the common problem of initializing a multi-step method.

This paper is organized as follows. In Section 2, we introduce the necessary notation and preliminary results needed in the proceeding sections. Section 3 introduces a second order AOT-DA scheme for the NSE, and proves stability, well-posedness, and long time accuracy, under typical regularity assumptions of the NSE solution. Section 4 contains three numerical tests that illustrate the convergence of the AOT-DA method, and issues that arise in numerical implementation that one may not see from the analysis.

# 2. Notation and preliminaries

We consider a bounded open domain  $\Omega \subset \mathbb{R}^d$  with d=2 or 3. The  $L^2(\Omega)$  norm and inner product will be denoted by  $\|\cdot\|$  and  $(\cdot, \cdot)$ , respectively, while all other norms will be labeled with subscripts.

Denote the natural function spaces for velocity and pressure, respectively, by

$$X := H_0^1(\Omega)^d$$
$$Q := L_0^2(\Omega).$$

In X, we have the Poincaré inequality: there exists a constant  $C_P$  depending only on  $\Omega$  such that for any  $\phi \in X$ ,

$$\|\phi\| \leq C_P \|\nabla\phi\|.$$

The dual norm of *X* will be denoted by  $\|\cdot\|_{-1}$ .

We denote the trilinear form  $b: X \times X \times X \to \mathbb{R}$ , which is defined on smooth functions u, v, w by

$$b(u, v, w) = \frac{1}{2}(u \cdot \nabla v, w) - \frac{1}{2}(u \cdot \nabla w, v).$$

An equivalent form of b on  $X \times X \times X$  can be constructed on smooth functions via

$$b(u,v,w) = (u \cdot \nabla v, w) + \frac{1}{2}((\nabla \cdot u)v, w).$$

An important property of the b operator is that b(u, v, v) = 0 for  $u, v \in X$ .

We will utilize the following bounds on b.

**Lemma 2.1.** There exists a constant M > 0 dependent only on  $\Omega$  satisfying

$$\begin{split} |b(u,v,w)| & \leq M \|\nabla u\| \|\nabla v\| \|\nabla w\|, \\ |b(u,v,w)| & \leq M \|u\| (\|\nabla v\|_{L^3} + \|v\|_{L^\infty}) \|\nabla w\|, \end{split}$$

for all  $u, v, w \in X$  for which the norms on the right hand sides are finite.

**Remark 2.2.** Here and throughout, sharper estimates are possible if we restrict to 2D. However, for simplicity and generality, we do not make this restriction.

**Proof.** These well known bounds follow from Hölder's inequality, Sobolev inequalities, and the Poincaré inequality.  $\Box$ 

# 2.1. Discretization preliminaries

Denote by  $\tau_h$  a regular, conforming triangulation of the domain  $\Omega$ , and let  $X_h \subset X$ ,  $Q_h \subset Q$  be an inf–sup stable pair of discrete velocity–pressure spaces. For simplicity, we will take  $X_h = X \cap P_k$  and  $Q_h = Q \cap P_{k-1}$  Taylor–Hood or Scott–Vogelius elements however our results in the following sections are extendable to most other inf–sup stable element choices.

We assume the mesh is sufficiently regular for the inverse inequality to hold: there exists a constant C such that for all  $v_h \in X_h$ ,

$$\|\nabla v_h\| \le Ch^{-1}\|v_h\|.$$

Define the discretely divergence free subspace by

$$V_h := \{v_h \in X_h \mid (\nabla \cdot v_h, q_h) = 0 \ \forall \ q_h \in Q_h\}.$$

For a given H > 0, we denote by  $I_H : X \to X$  a linear operator satisfying

$$||I_H(\phi) - \phi|| \le C_I H ||\nabla \phi||, \tag{2.3}$$

$$||I_H(\phi)|| \le C||\phi||,\tag{2.4}$$

for some  $C \ge 1$ , and for all  $\phi \in X$ . For example,  $I_H$  could be an appropriate interpolation operator such as a nodal interpolant on  $X \cap P_k(\tau_H)$  with  $k \ge 1$ , or an appropriate projection operator such as the  $L^2$  projection onto  $P_0(\tau_H)$  [36]. Here, H is a characteristic point spacing, and will satisfy  $h \le H$ , H = ch. The spacing H corresponds in practice to points where (true solution) measurements are taken, so H should be as large as possible but still satisfying (2.3)–(2.4).

Throughout this paper, we make the assumption on the mesh width h that it satisfies the data dependent restriction

$$h < \sqrt{\frac{2\nu}{C_I^2 C(\text{data}, u)}}.$$

This will allow for choosing nudging parameters  $\mu$  in the interval  $(C(\text{data}, u), \frac{v}{2}C_I^{-2}h^{-2})$ .

We also define the quantity

$$\alpha := \nu - 2\mu C_I^2 h^2$$
,

and will assume that  $\alpha > 0$ . Note that  $\mu$  will also have a data dependent lower bound in our analysis, but choosing h small enough will allow an appropriate  $\mu$  to be chosen.

# 2.2. Additional preliminaries

Several results in this paper utilize the following inequality for sequences.

**Lemma 2.5.** Suppose constants r and B satisfy r > 1,  $B \ge 0$ . Then if the sequence of real numbers  $\{a_n\}$  satisfies

$$ra_{n+1} < a_n + B,$$
 (2.6)

we have that

$$a_{n+1} \le a_0 \left(\frac{1}{r}\right)^{n+1} + \frac{B}{r-1}.$$

**Proof.** The inequality (2.6) can be written as

$$a_{n+1} \le \frac{a_n}{r} + \frac{B}{r}.$$

Recursively, we obtain

$$a_{n+1} \le \frac{1}{r} \left( \frac{a_{n-1}}{r} + \frac{B}{r} \right) + \frac{B}{r}$$

$$= \frac{a_{n-1}}{r^2} + \frac{B}{r} \left( 1 + \frac{1}{r} \right)$$

$$\vdots$$

$$\le \frac{a_0}{r^{n+1}} + \frac{B}{r} \left( 1 + \frac{1}{r} + \dots + \frac{1}{r^n} \right).$$

Now the resulting finite geometric series is bounded as

$$\frac{B}{r}\left(1+\frac{1}{r}+\dots+\frac{1}{r^n}\right) = \frac{B}{r}\cdot\frac{1-(1/r)^{n+1}}{1-(1/r)} \le \frac{B}{r}\cdot\frac{1}{1-(1/r)} \le \frac{B}{r-1},$$

which gives the result.  $\square$ 

The analysis in Section 3 uses a BDF2 approximation to the time derivative term will use the G-norm, which is commonly used in BDF2 analysis, see e.g. [37,38]. Define the matrix

$$G = \begin{bmatrix} 1/2 & -1 \\ -1 & 5/2 \end{bmatrix},$$

and note that G induces the norm  $||x||_G^2 := (x, Gx)$ , which is equivalent to the  $(L^2)^2$  norm:

$$C_l ||x||_G \le ||x|| \le C_u ||x||_G$$

where  $C_l = 3 - 2\sqrt{2}$  and  $C_u = 3 + 2\sqrt{2}$ . The following property is well-known [37]. Set  $\chi_v^n := [v^{n-1}, v^n]^T$ , if  $v^i \in L^2(\Omega)$ , i = n - 1, n, we have

$$\left(\frac{1}{2}(3v^{n+1} - 4v^n + v^{n-1}), v^{n+1}\right) = \frac{1}{2}(\|\chi_v^{n+1}\|_G^2 - \|\chi_v^n\|_G^2) + \frac{1}{4}\|v^{n+1} - 2v^n + v^{n-1}\|^2.$$
(2.7)

### 3. A second order IMEX FEM scheme and its analysis

We consider now an efficient fully discretized scheme for (1.3)–(1.4). We use the second order BDF2 temporal discretization, and the scheme is linearized at each time step by extrapolating part of the convective term from previous time solutions. The spatial discretization is the finite element method, and we assume the velocity–pressure finite element spaces  $(X_h, Q_h) = (P_k, P_{k-1})$  for simplicity, although extension to any Ladyzhenskaya–Babuska–Brezzi (LBB)-stable pair can be done without significant difficulty. We also utilize grad-div stabilization, with parameter  $\gamma > 0$ , and assume  $\gamma = O(1)$ . For most common element choices, grad-div stabilization is known to improve mass conservation and reduce the effect of the pressure on the velocity error [39]; a similar effect is observed in the convergence result for this AOT-DA scheme, as well as in the numerical tests. In this section, we prove well-posedness, and global-in-time stability and convergence for a wide range of possible values for the nudging parameter the time step size. We note that analogous results can be proven for the case of backward Euler time stepping, using similar analysis. The second order IMEX-FEM AOT-DA algorithm is defined as follows.

**Algorithm 3.1.** Given any initial conditions  $v_h^0$ ,  $v_h^1 \in V_h$ , forcing  $f \in L^{\infty}(0, \infty; L^2(\Omega))$ , true solution  $u \in L^{\infty}(0, \infty; L^2(\Omega))$ , grad-div parameter  $\gamma > 0$ ,  $I_H$  satisfying (2.3)–(2.4), and nudging parameter  $\mu > 0$ , find  $(v_h^{n+1}, q_h^{n+1}) \in (X_h, Q_h)$  for  $n = 1, 2, \ldots$ , satisfying

$$\frac{1}{2\Delta t} \left( 3v_h^{n+1} - 4v_h^n + v_h^{n-1}, \chi_h \right) + b(2v_h^n - v_h^{n-1}, v_h^{n+1}, \chi_h) - (q_h^{n+1}, \nabla \cdot \chi_h) 
+ \gamma(\nabla \cdot v_h^{n+1}, \nabla \cdot \chi_h) + \nu(\nabla v_h^{n+1}, \nabla \chi_h) + \mu(I_H(v_h^{n+1} - u^{n+1}), \chi_h) = (f^{n+1}, \chi_h),$$
(3.1)

$$(\nabla \cdot v_h^{n+1}, r_h) = 0, \tag{3.2}$$

for all  $(\chi_h, r_h) \in X_h \times Q_h$ .

**Remark 3.3.** We show below that under some regularity assumptions on the true solution u, the AOT-DA algorithm converges to u as  $t \to \infty$ , independent of the initial conditions. Thus, the initial conditions can be chosen arbitrarily, although more accurate initial conditions may reduce the time to convergence to the true solution.

Well-posedness and long time stability of this algorithm are achieved by using G-stability theory on the time derivative terms. We state and prove this result now.

**Lemma 3.4.** Assume h satisfies  $0 < h < \frac{\sqrt{\nu}}{C_I \sqrt{2}}$  and  $0 < \mu < \frac{\nu}{2C_I^2 h^2}$ . Then for any  $\Delta t > 0$ , Algorithm 3.1 is well-posed globally in time, and solutions are nonlinearly long-time stable: for any n > 1,

$$\begin{split} & \left( C_l^2 \left( \| v_h^{n+1} \|^2 + \| v_h^n \|^2 \right) + \frac{\alpha \Delta t}{4} \| \nabla v_h^{n+1} \|^2 + \frac{\mu \Delta t}{4} \| v_h^{n+1} \|^2 \right) \\ & \leq \left( C_u^2 \| v_h^1 \|^2 + \| v_h^0 \|^2 + \frac{\alpha \Delta t}{4} \| \nabla v_h^1 \|^2 + \frac{\mu \Delta t}{4} \| v_h^1 \|^2 \right) \left( \frac{1}{1 + \lambda \Delta t} \right)^{n+1} + C \lambda^{-1} v^{-1} F^2 + C \lambda^{-1} \mu U^2. \end{split}$$

where  $\lambda = \min\{\frac{\mu C_l^2}{4}, \frac{\alpha C_p^{-2} C_l^2}{4}, 2\Delta t^{-1}\}$ ,  $U := \|u\|_{L^{\infty}(0,\infty;L^2)}$ , and  $F := \|f\|_{L^{\infty}(0,\infty;H^{-1})}$ .

**Proof.** Choose  $\chi_h = v_h^{n+1}$  in (3.1) and use (2.7) to obtain the bound

$$\frac{1}{2\Delta t} \left( \| [v_h^{n+1}; v_h^n] \|_G^2 \right) + \nu \| \nabla v_h^{n+1} \|^2 + \mu(I_H(v_h^{n+1}), v_h^{n+1}) \\
\leq \frac{1}{2\Delta t} \left( \| [v_h^n; v_h^{n-1}] \|_G^2 \right) + |(f^{n+1}, v_h^{n+1})| + \mu|(I_H(u^{n+1}), v_h^{n+1})|,$$

noting that we dropped the non-negative terms  $\gamma \|\nabla \cdot v_h^{n+1}\|^2$  and  $\frac{1}{4\Delta t} \|v_h^{n+1} - 2v_h^n + v_h^{n-1}\|^2$  from the left hand side, and that the nonlinear term and pressure term drop due to the choice of test function. We next add and subtract  $v_h^{n+1}$  in the first component of the nudging term so that the above bound becomes

$$\frac{1}{2\Delta t} \left( \| [v_h^{n+1}; v_h^n] \|_G^2 \right) + \nu \| \nabla v_h^{n+1} \|^2 + \mu \| v_h^{n+1} \|^2 
\leq \frac{1}{2\Delta t} \left( \| [v_h^n; v_h^{n-1}] \|_G^2 \right) + | (f^{n+1}, v_h^{n+1})| + \mu | (I_H v_h^{n+1} - v_h^{n+1}, v_h^{n+1})| + \mu | (I_H (u^{n+1}), v_h^{n+1})|.$$
(3.5)

The first term on the right hand side is bounded using the dual norm of X and Young's inequality, which yields

$$|(f^{n+1}, v_h^{n+1})| \le ||f^{n+1}||_{-1} ||\nabla v_h^{n+1}|| \le \frac{v^{-1}}{2} ||f^{n+1}||_{-1}^2 + \frac{v}{2} ||\nabla v_h^{n+1}||^2.$$

The second right hand side term is bounded using Cauchy–Schwarz, interpolation property (2.3), and Young's inequality, after which we have that

$$\begin{split} \mu|(I_Hv_h^{n+1}-v_h^{n+1},v_h^{n+1})| &\leq \mu\|I_Hv_h^{n+1}-v_h^{n+1}\|\|v_h^{n+1}\|\\ &\leq \mu C_I^2h^2\|\nabla v_h^{n+1}\|^2 + \frac{\mu}{4}\|v_h^{n+1}\|^2. \end{split}$$

Finally, the last right hand side term will be bounded with these same inequalities, and property (2.4), to obtain

$$\begin{split} \mu(I_H u^{n+1}, v_h^{n+1}) &\leq \mu \|I_H u^{n+1}\| \|v_h^{n+1}\| \\ &\leq C \mu \|u^{n+1}\|^2 + \frac{\mu}{4} \|v_h^{n+1}\|^2. \end{split}$$

Now majorize the right hand side of (3.5) with these computed bounds, multiply both sides by  $2\Delta t$ , and then reduce to obtain

$$\|[v_h^{n+1}; v_h^n]\|_G^2 + \alpha \Delta t \|\nabla v_h^{n+1}\|^2 + \mu \Delta t \|v_h^{n+1}\|^2 \le \|[v_h^n; v_h^{n-1}]\|_G^2 + \Delta t (v^{-1}F^2 + C\mu U^2).$$

Next, adding  $\frac{\mu \Delta t}{4} \|v_h^n\|^2 + \frac{\alpha \Delta t}{4} \|\nabla v_h^n\|^2$  to both sides and rearranging gives

$$\begin{split} \left( \| [v_h^{n+1}; \, v_h^n] \|_G^2 + \frac{\mu \, \Delta t}{4} \| v_h^{n+1} \|^2 + \frac{\alpha \, \Delta t}{4} \| \nabla v_h^{n+1} \|^2 \right) \\ + \frac{\mu \, \Delta t}{4} \left( \| v_h^{n+1} \|^2 + \| v_h^n \|^2 \right) + \frac{\alpha \, \Delta t}{4} \left( \| \nabla v_h^{n+1} \|^2 + \| \nabla v_h^n \|^2 \right) + \frac{\mu \, \Delta t}{2} \| v_h^{n+1} \|^2 + \frac{\alpha \, \Delta t}{2} \| \nabla v_h^{n+1} \|^2 \\ \leq \left( \| [v_h^n; \, v_h^{n-1}] \|_G^2 + \frac{\mu \, \Delta t}{4} \| v_h^n \|^2 + \frac{\alpha \, \Delta t}{4} \| \nabla v_h^n \|^2 \right) + \Delta t (v^{-1} F^2 + C \mu U^2), \end{split}$$

which reduces using Poincaré's inequality and G-norm equivalence to

$$\begin{split} \left( \| [v_h^{n+1}; \, v_h^n] \|_G^2 + \frac{\mu \Delta t}{4} \| v_h^{n+1} \|^2 + \frac{\alpha \Delta t}{4} \| \nabla v_h^{n+1} \|^2 \right) \\ + \frac{\mu \Delta t C_l^2}{4} \| [v_h^{n+1}; \, v_h^n] \|_G^2 + \frac{\alpha \Delta t C_P^{-2} C_l^2}{4} \| [v_h^{n+1}; \, v_h^n] \|_G^2 + \frac{\mu \Delta t}{2} \| v_h^{n+1} \|^2 + \frac{\alpha \Delta t}{2} \| \nabla v_h^{n+1} \|^2 \\ \leq \left( \| [v_h^n; \, v_h^{n-1}] \|_G^2 + \frac{\mu \Delta t}{4} \| v_h^n \|^2 + \frac{\alpha \Delta t}{4} \| \nabla v_h^n \|^2 \right) + \Delta t (v^{-1} F^2 + C \mu U^2). \end{split}$$

Thus there exists  $\lambda=\min\{\frac{\mu C_l^2}{l},\,\frac{\alpha C_P^{-2}C_l^2}{2l},\,\frac{2}{\Delta t}\}$  such that

$$(1 + \lambda \Delta t) \left( \| [v_h^{n+1}; v_h^n] \|_G^2 + \frac{\alpha \Delta t}{4} \| \nabla v_h^{n+1} \|^2 + \frac{\mu \Delta t}{4} \| v_h^{n+1} \|^2 \right)$$

$$\leq \left( \| [v_h^n; v_h^{n-1}] \|_G^2 + \frac{\alpha \Delta t}{4} \| \nabla v_h^n \|^2 + \frac{\mu \Delta t}{4} \| v_h^n \|^2 \right) + \Delta t (v^{-1} F^2 + C \mu U^2),$$

and so by Lemma 2.5,

$$\begin{split} \left( \| [v_h^{n+1}; v_h^n] \|_G^2 + \frac{\alpha \Delta t}{4} \| \nabla v_h^{n+1} \|^2 + \frac{\mu \Delta t}{4} \| v_h^{n+1} \|^2 \right) \\ & \leq \left( \| [v_h^1; v_h^0] \|_G^2 + \frac{\alpha \Delta t}{4} \| \nabla v_h^1 \|^2 + \frac{\mu \Delta t}{4} \| v_h^1 \|^2 \right) \left( \frac{1}{1 + \lambda \Delta t} \right)^{n+1} \\ & + C \lambda^{-1} (v^{-1} F^2 + \mu U^2). \end{split}$$

Applying the G-norm equivalence completes the proof of stability.

Since the scheme is linear and finite dimensional at each time step, this uniform in n stability result gives existence and uniqueness of the algorithm at every time step.  $\Box$ 

**Corollary 3.6.** For the case of  $I_H$  chosen as the  $L^2$  projection onto piecewise constants  $P_0(\tau_H)$ , long time  $L^2$  stability (and well-posedness) holds for any  $\mu < \infty$ .

**Proof.** Following the same analysis as above except for the nudging term which can be handled in this case as

$$\begin{split} \mu(P_{L^2}^{P_0}(v_h^{n+1}-u^{n+1}),v_h^{n+1}) &= \mu(P_{L^2}^{P_0}(v_h^{n+1}-u^{n+1}),P_{L^2}^{P_0}v_h^{n+1}) \\ &= \frac{\mu}{2} \left( \|P_{L^2}^{P_0}v_h^{n+1}\|^2 - \|P_{L^2}^{P_0}u^{n+1}\|^2 + \|P_{L^2}^{P_0}(v_h^{n+1}-u^{n+1})\|^2 \right), \end{split}$$

we obtain

$$\begin{split} &\frac{1}{\Delta t} \left( \|[v_h^{n+1}; \, v_h^n]\|_G^2 \right) + \nu \|\nabla v_h^{n+1}\|^2 + \mu \|P_{L^2}^{P_0} v_h^{n+1}\|^2 + \mu \|P_{L^2}^{P_0} (v_h^{n+1} - u^{n+1})\|^2 \\ &\leq \frac{1}{\Delta t} \left( \|[v_h^n; \, v_h^{n-1}]\|_G^2 \right) + \mu \|P_{L^2}^{P_0} u^{n+1}\|^2 + \nu^{-1} \|f^{n+1}\|_{-1}^2. \end{split}$$

From here, similar analysis as above will prove a long time  $L^2$  stability result similar to that in the theorem above.  $\Box$ 

We now prove that solutions to Algorithm 3.1 converge to the true NSE solution at a rate of  $\Delta t^2 + h^k$ , globally in time, provided restrictions on  $\Delta t$  and  $\mu$  are satisfied. The time derivative term will again be handled with the G-stability theory in a manner similar to the stability proof.

**Theorem 3.7.** Let u, p solve the NSE (1.1)– (1.2) with given  $f \in L^{\infty}(0, \infty; L^{2}(\Omega))$  and  $u_{0} \in L^{2}(\Omega)$ , with  $u \in L^{\infty}(0, \infty; H^{k+1}(\Omega))$ ,  $p \in L^{\infty}(0, \infty; H^{k}(\Omega))$   $(k \ge 1)$ ,  $u_{tt} \in L^{\infty}(0, \infty; L^{2}(\Omega))$ , and  $u_{ttt} \in L^{\infty}(0, \infty; H^{1}(\Omega))$ . Denote  $U := |u|_{L^{\infty}(0,\infty;H^{k+1})}$  and  $P := |p|_{L^{\infty}(0,\infty;H^{k})}$ . Assume the time step size satisfies

$$\Delta t < CM^2 \nu^{-1} \left( h^{2k-3} U^2 + \|\nabla u^{n+1}\|_{L^3}^2 + \|u^{n+1}\|_{L^\infty}^2 \right)^{-1},$$

and the parameter  $\mu$  satisfies

$$CM^{2}\nu^{-1}\left(h^{2k-3}U^{2}+\|\nabla u^{n+1}\|_{L^{3}}^{2}+\|u^{n+1}\|_{L^{\infty}}^{2}\right)<\mu<\frac{2\nu}{C_{I}^{2}h^{2}}.$$

Then the error in solutions to Algorithm 3.1 satisfies, for any n,

$$\|u^n - v_h^n\|^2 \le C \left(\frac{1}{1 + \lambda \Delta t}\right)^n \|u_0 - v_h^0\|^2 + \frac{R}{\lambda},$$

where 
$$R = Cv^{-1}(1+M^2)\Delta t^4 + Ch^{2k}\left(\gamma^{-1}P^2 + (v+\gamma+M^2v^{-1}+M^2v^{-1}h^{2k}U^2 + vC_I^{-2})U^2\right)$$
 and  $\lambda = 2C_I^2\alpha C_P^{-2}$ .

**Remark 3.8.** The restrictions on h and  $\mu$  are sufficient conditions under which convergence of the algorithm will be guaranteed, and with the error estimate given above. It is entirely possible that convergence of the AOT-DA algorithm can happen for  $\mu$  chosen outside of this range (and if so, potentially with a different error estimate), and our numerical experiments suggest this might be true, in particular for the case of large  $\mu$ . Proving such a result would seemingly require a different approach to the analysis than we take in the proof below.

**Remark 3.9.** For the case of Taylor–Hood  $(P_2, P_1)$  or Scott–Vogelius  $(P_2, P_1^{disc})$  elements and 0 initial condition in the AOT-DA algorithm, the result of this theorem reduces to

$$||u^n - v_h^n|| \le C \left( \left( \frac{1}{1 + \lambda \Delta t} \right)^{n/2} ||u_0|| + \Delta t^2 + h^2 \right),$$

where C depends on problem data and the true solution, but not  $\Delta t$  or h.

**Remark 3.10.** The time step restriction is a consequence of the IMEX time stepping. If we instead consider the fully nonlinear scheme, i.e. with  $b(2v_h^n - v_h^{n-1}, v_h^{n+1}, \chi_h)$  replaced by  $b(v_h^{n+1}, v_h^{n+1}, \chi_h)$ , then no  $\Delta t$  restriction is required for a similar result to hold. However, in this case a time step restriction seemingly becomes necessary for solution uniqueness of the nonlinear scheme.

**Remark 3.11.** Similar to the case of NSE-FEM without AOT-DA, grad-div stabilization reduces the effect of the pressure on the  $L^2(\Omega)$  AOT-DA solution error. With grad-div, the contribution of the pressure to the error is  $h^k \gamma^{-1/2} |p|_{L^\infty(0,\infty;H^k)}$ , but without it, the  $\gamma^{-1/2}$  is be replaced by a  $\nu^{-1/2}$ . If divergence-free elements were used, then this term completely vanishes, since in the proof below in (3.17) we would obtain  $(p^{n+1} - r_h, \nabla \cdot \phi_h^{n+1}) = 0$  and thus no pressure terms would appear in the final estimate.

**Proof.** Throughout this proof, the constant C will denote a generic constant, possibly changing from line to line, that is independent of h,  $\mu$ , and  $\Delta t$ .

Using Taylor's theorem, the NSE (true) solution satisfies, for all  $\chi_h \in X_h$ ,

$$\frac{1}{2\Delta t} \left( 3u^{n+1} - 4u^n + u^{n-1}, \chi_h \right) + b(2u^n - u^{n-1}, u^{n+1}, \chi_h) - (p^{n+1}, \nabla \cdot \chi_h) + \gamma(\nabla \cdot u^{n+1}, \nabla \cdot \chi_h) 
+ \nu(\nabla u^{n+1}, \nabla \chi_h) = (f^{n+1}, \chi_h) + \frac{\Delta t^2}{3} (u_{ttt}(t^*), \chi_h) + \Delta t^2 b(u_{tt}(t^{**}), u^{n+1}, \chi_h),$$
(3.12)

where  $t^*, t^{**} \in [t^{n-1}, t^{n+1}]$ . Subtracting (3.1) from (3.12) yields the following difference equation, with  $e^n := u^n - v_h^n$ :

$$\frac{1}{2\Delta t}(3e^{n+1} - 4e^n + e^{n-1}, \chi_h) + \nu(\nabla e^{n+1}, \nabla \chi_h) + \mu(I_H(e^{n+1}), \chi_h) + \gamma(\nabla \cdot e^{n+1}, \nabla \cdot \chi_h) \\
= \frac{\Delta t^2}{3}(u_{ttt}(t^*), \chi_h) + \Delta t^2(u_{tt}(t^{**}) \cdot \nabla u^{n+1}, \chi_h) - (p^{n+1}, \nabla \cdot \chi_h) + b(2v_h^n - v_h^{n-1}, e^{n+1}, \chi_h) \\
+ b(2e^n - e^{n-1}, u^{n+1}, \chi_h).$$

We decompose the error into a piece inside the discrete space  $V_h$  and one outside of it by adding and subtracting  $P_{V_h}^{L^2}(u^n)$ . Denote  $\eta^n := u^n - P_{V_h}^{L^2}(u^n)$  and  $\phi_h^n := P_{V_h}^{L^2}(u^n) - v_h^n$ . Then  $e^n = \eta^n + \phi_h^n$  with  $\phi_h^n \in V_h$ , and we choose  $\chi_h = \phi_h^{n+1}$ . Using identity (2.7) with  $\psi_\phi := (\phi_h^n, \phi_h^{n+1})^T$ , the difference equation becomes

$$\frac{1}{2\Delta t} [\|\psi_{\phi}^{n+1}\|_{G}^{2} - \|\psi_{\phi}^{n}\|_{G}^{2}] + \frac{1}{4\Delta t} \|\phi_{h}^{n+1} - 2\phi_{h}^{n} + \phi_{h}^{n-1}\|^{2} + \nu \|\nabla\phi_{h}^{n+1}\|^{2} + \mu \|\phi_{H}^{n+1}\|^{2} + \gamma \|\nabla\cdot\phi_{h}^{n+1}\|^{2} 
= \frac{\Delta t^{2}}{3} (u_{ttt}(t^{*}), \phi_{h}^{n+1}) + \Delta t^{2} (u_{tt}(t^{**}) \cdot \nabla u^{n+1}, \phi_{h}^{n+1}) - (p^{n+1}, \nabla\cdot\phi_{h}^{n+1}) 
+ b(2\phi_{h}^{n} - \phi_{h}^{n-1}, u^{n+1}, \phi_{h}^{n+1}) + b(2\eta^{n} - \eta^{n-1}, u^{n+1}, \phi_{h}^{n+1}) + b(2v_{h}^{n} - v_{h}^{n-1}, \eta^{n+1}, \phi_{h}^{n+1}) 
- \nu(\nabla\eta^{n+1}, \nabla\phi_{h}^{n+1}) - \mu(I_{H}\phi_{h}^{n+1} - \phi_{h}^{n+1}, \phi_{h}^{n+1}) - \mu(I_{H}\eta^{n+1}, \phi_{h}^{n+1}) 
- \gamma(\nabla\cdot\eta^{n+1}, \nabla\cdot\phi_{h}^{n+1}),$$
(3.13)

where we have added and subtracted  $\phi_h^{n+1}$  in the interpolation term on the left hand side. We can now bound the right hand side of (3.13). Many of these terms are bounded in a similar manner as in the case of BDF2 FEM for NSE, for example as in [40–42]. We will use these techniques (which mainly consist of carefully constructed Young and Cauchy–Schwarz inequalities and Lemma 2.1) to bound all terms except the nonlinear and nudging terms. For the first nonlinear term in (3.13), we add and subtract  $\phi_h^{n+1}$  in the first argument to obtain

$$b(2\phi_h^n - \phi_h^{n-1}, u^{n+1}, \phi_h^{n+1}) = b(\phi_h^{n+1}, u^{n+1}, \phi_h^{n+1}) - b(\phi_h^{n+1} - 2\phi_h^n + \phi_h^{n-1}, u^{n+1}, \phi_h^{n+1}). \tag{3.14}$$

We bound the two resulting terms using Lemma 2.1 and Young's inequality, via

$$b(\phi_h^{n+1}, u^{n+1}, \phi_h^{n+1}) \leq CM v^{-1} (\|\nabla u^{n+1}\|_{L^3}^2 + \|u^{n+1}\|_{L^\infty}^2) \|\phi_h^{n+1}\|^2 + \frac{v}{16} \|\nabla \phi_h^{n+1}\|^2,$$

and

$$\begin{split} b(\phi_h^{n+1} - 2\phi_h^n + \phi_h^{n-1}, u^{n+1}, \phi_h^{n+1}) \\ & \leq C M v^{-1} (\|\nabla u^{n+1}\|_{L^3}^2 + \|u^{n+1}\|_{L^\infty}^2) \|\phi_h^{n+1} - 2\phi_h^n + \phi_h^{n-1}\|^2 + \frac{v}{16} \|\nabla \phi_h^{n+1}\|^2. \end{split}$$

The second nonlinear term in (3.13) is bounded with this same technique:

$$\begin{split} b(2\eta^n - \eta^{n-1}, u^{n+1}, \phi_h^{n+1}) \\ & \leq C M^2 \nu^{-1} (\|\nabla u^{n+1}\|_{L^3}^2 + \|u^{n+1}\|_{L^\infty}^2) \|2\eta^n - \eta^{n-1}\|^2 + \frac{\nu}{16} \|\nabla \phi_h^{n+1}\|^2. \end{split}$$

The last nonlinear term in (3.13) requires a bit more work, and we start by adding and subtracting  $2u^n - u^{n-1}$  in the first component, which yields

$$b(2v_{h}^{n} - v_{h}^{n-1}, \eta^{n+1}, \phi_{h}^{n+1}) = b(2u^{n} - u^{n-1}, \eta^{n+1}, \phi_{h}^{n+1}) + b(2e^{n} - e^{n-1}, \eta^{n+1}, \phi_{h}^{n+1})$$

$$= b(2u^{n} - u^{n-1}, \eta^{n+1}, \phi_{h}^{n+1}) + b(2\phi_{h}^{n} - \phi_{h}^{n-1}, \eta^{n+1}, \phi_{h}^{n+1})$$

$$+ b(2\eta^{n} - \eta^{n-1}, \eta^{n+1}, \phi_{h}^{n+1}).$$
(3.15)

The first and third terms on the right hand side of (3.15) are bounded in the same way, using Lemma 2.1 and Young's inequality, we find

$$b(2u^{n}-u^{n-1},\eta^{n+1},\phi_{h}^{n+1}) \leq Cv^{-1}M^{2}\|\nabla(2u^{n}-u^{n-1})\|^{2}\|\nabla\eta^{n+1}\|^{2} + \frac{v}{16}\|\nabla\phi_{h}^{n+1}\|^{2},$$

$$b(2\eta^{n} - \eta^{n-1}, \eta^{n+1}, \phi_{h}^{n+1}) \leq C\nu^{-1}M^{2}\|\nabla(2\eta^{n} - \eta^{n-1})\|^{2}\|\nabla\eta^{n+1}\|^{2} + \frac{\nu}{16}\|\nabla\phi_{h}^{n+1}\|^{2}.$$

For the second term in (3.15) we first add  $\phi_h^{n+1}$  to the first argument to obtain

$$b(2\phi_h^n - \phi_h^{n-1}, \eta^{n+1}, \phi_h^{n+1}) = b(\phi_h^{n+1} - 2\phi_h^n + \phi_h^{n-1}, \eta^{n+1}, \phi_h^{n+1}) + b(\phi_h^{n+1}, \eta^{n+1}, \phi_h^{n+1}),$$

and then bound each resulting term using Lemma 2.1 and Young's inequality:

$$b(\phi_h^{n+1},\eta^{n+1},\phi_h^{n+1}) \leq CM^2 \nu^{-1} (\|\eta^{n+1}\|_{L^{\infty}}^2 + \|\nabla \eta^{n+1}\|_{L^3}^2) \|\phi_h^{n+1}\|^2 + \frac{\nu}{16} \|\nabla \phi_h^{n+1}\|^2,$$

$$\begin{split} b(\phi_h^{n+1} - 2\phi_h^n + \phi_h^{n-1}, \eta^{n+1}, \phi_h^{n+1}) \\ & \leq CM^2 \nu^{-1} (\|\eta^{n+1}\|_{L^\infty}^2 + \|\nabla \eta^{n+1}\|_{L^3}^2) \|\phi_h^{n+1} - 2\phi_h^n + \phi_h^{n-1}\|^2 + \frac{\nu}{16} \|\nabla \phi_h^{n+1}\|^2. \end{split}$$

For the first nudging term in (3.13), we apply Cauchy-Schwarz and Young's inequalities and (2.3) to obtain

$$\begin{split} \mu \left| (I_{H}(\phi_{h}^{n+1}) - \phi_{h}^{n+1}, \phi_{h}^{n+1}) \right| &\leq \mu \|I_{H}(\phi_{h}^{n+1}) - \phi_{h}^{n+1}\| \|\phi_{h}^{n+1}\| \\ &\leq \mu C_{I} h \|\nabla \phi_{h}^{n+1}\| \|\phi_{h}^{n+1}\| \\ &\leq \mu C_{I}^{2} h^{2} \|\nabla \phi_{h}^{n+1}\|^{2} + \frac{\mu}{4} \|\phi_{h}^{n+1}\|^{2}. \end{split}$$

Finally, for the last nudging term in (3.13), we employ Cauchy–Schwarz and Young inequalities, along with (2.4), to obtain

$$\mu(I_{H}(\eta^{n+1}), \phi_{h}^{n+1}) \leq \mu \|I_{H}(\eta^{n+1})\| \|\phi_{h}^{n+1}\|$$

$$\leq C\mu \|\eta^{n+1}\|^{2} + \frac{\mu}{4} \|\phi_{h}^{n+1}\|^{2}.$$

Collecting the above bounds, we reduce (3.13) to

$$\begin{split} &\frac{1}{2\Delta t}[\|\psi_{\phi}^{n+1}\|_{G}^{2} - \|\psi_{\phi}^{n}\|_{G}^{2}] + \frac{9\nu}{16}\|\nabla\phi_{h}^{n+1}\|^{2} + \gamma\|\nabla\cdot\phi_{h}^{n+1}\|^{2} \\ &+ \left(\frac{1}{4\Delta t} - CM^{2}\nu^{-1}(\|\eta^{n+1}\|_{L^{\infty}}^{2} + \|\nabla\eta^{n+1}\|_{L^{3}}^{2} + \|u^{n+1}\|_{L^{\infty}}^{2} + \|\nabla u^{n+1}\|^{2})\right)\|\phi_{h}^{n+1} - 2\phi_{h}^{n} + \phi_{h}^{n-1}\|^{2} \\ &+ \left(\mu - CM^{2}\nu^{-1}(\|\eta^{n+1}\|_{L^{\infty}}^{2} + \|\nabla\eta^{n+1}\|_{L^{3}}^{2} + \|u^{n+1}\|_{L^{\infty}}^{2} + \|\nabla u^{n+1}\|^{2})\right)\|\phi_{h}^{n+1}\|^{2} \\ &\leq C\Delta t^{2}\|u_{ttt}\|_{L^{\infty}(t^{n-1},t^{n+1},L^{2})}\|\phi_{h}^{n+1}\| + \Delta t^{2}|(u_{tt}(t^{**})\cdot\nabla u^{n+1},\phi_{h}^{n+1})| + |(p^{n+1}-r_{h},\nabla\cdot\phi_{h}^{n+1})| \\ &+ \nu|(\nabla\eta^{n+1},\nabla\phi_{h}^{n+1})| + \mu|(I_{H}\phi_{h}^{n+1}-\phi_{h}^{n+1},\phi_{h}^{n+1})| + \mu|(I_{H}\eta^{n+1},\phi_{h}^{n+1})| \\ &+ C\nu^{-1}M^{2}\|\nabla(2u^{n}-u^{n-1})\|^{2}\|\nabla\eta^{n+1}\|^{2} + C\nu^{-1}M^{2}\|\nabla(2\eta^{n}-\eta^{n-1})\|^{2}\|\nabla\eta^{n+1}\|^{2} \\ &+ CM^{2}\nu^{-1}(\|\nabla u^{n+1}\|_{L^{3}}^{2} + \|u^{n+1}\|_{L^{\infty}}^{2})\|2\eta^{n}-\eta^{n-1}\|^{2} + \gamma|(\nabla\cdot\eta^{n+1},\nabla\cdot\phi_{h}^{n+1})|, \end{split} \tag{3.16}$$

where  $r_h \in Q_h$  is chosen arbitrarily, see e.g. [43]. Now using interpolation estimates (and implicitly also the inverse inequality) along with regularity assumptions, we obtain

$$\frac{1}{2\Delta t} [\|\psi_{\phi}^{n+1}\|_{G}^{2} - \|\psi_{\phi}^{n}\|_{G}^{2}] + \frac{9\nu}{16} \|\nabla\phi_{h}^{n+1}\|^{2} + \gamma \|\nabla\cdot\phi_{h}^{n+1}\|^{2} 
+ \left(\frac{1}{4\Delta t} - CM^{2}\nu^{-1}(h^{2k-3}U^{2} + \|u^{n+1}\|_{L^{\infty}}^{2} + \|\nabla u^{n+1}\|_{L^{3}}^{2})\right) \|\phi_{h}^{n+1} - 2\phi_{h}^{n} + \phi_{h}^{n-1}\|^{2} 
+ \left(\mu - CM^{2}\nu^{-1}(h^{2k-3}U^{2} + \|u^{n+1}\|_{L^{\infty}}^{2} + \|\nabla u^{n+1}\|_{L^{3}}^{2})\right) \|\phi_{h}^{n+1}\|^{2} 
\leq C\Delta t^{2} \|u_{ttt}\|_{L^{\infty}(t^{n-1},t^{n+1},L^{2})} \|\phi_{h}^{n+1}\| + \Delta t^{2} |(u_{tt}(t^{**})\cdot\nabla u^{n+1},\phi_{h}^{n+1})| 
+ |(p^{n+1} - r_{h},\nabla\cdot\phi_{h}^{n+1})| + \nu |(\nabla\eta^{n+1},\nabla\phi_{h}^{n+1})| + \mu |(I_{H}\phi_{h}^{n+1} - \phi_{h}^{n+1},\phi_{h}^{n+1})| 
+ \mu |(I_{H}\eta^{n+1},\phi_{h}^{n+1})| + CM^{2}\nu^{-1}h^{2k}U^{2}(1 + h^{2k}U^{2}) + \gamma |(\nabla\cdot\eta^{n+1},\nabla\cdot\phi_{h}^{n+1})|.$$
(3.17)

Next we use the assumptions on  $\Delta t$  and  $\mu$ , and apply bounds to the remaining right hand side terms similar to NSE convergence analyses in [41] to find

$$\frac{1}{2\Delta t} [\|\psi_{\phi}^{n+1}\|_{G}^{2} - \|\psi_{\phi}^{n}\|_{G}^{2}] + \alpha \|\nabla\phi_{h}^{n+1}\|^{2} + \frac{\gamma}{2} \|\nabla\cdot\phi_{h}^{n+1}\|^{2} 
\leq C\nu^{-1}(1+M^{2})\Delta t^{4} + Ch^{2k} \left(\gamma^{-1}P^{2} + (\nu+\gamma+M^{2}\nu^{-1}+M^{2}\nu^{-1}h^{2k}U^{2} + \nu C_{I}^{-2})U^{2}\right) 
=: R.$$
(3.18)

This implies, with Poincaré's inequality that

$$\|\psi_{\phi}^{n+1}\|_{G}^{2}+2C_{l}^{2}\Delta t\alpha C_{P}^{-2}\|\phi_{h}^{n+1}\|^{2}\leq\|\psi_{\phi}^{n}\|_{G}^{2}+\Delta tR.$$

From here, we can proceed just as in to the BDF2 long time stability proof above to obtain

$$\|\psi_{\phi}^{n+1}\|_{G}^{2} \leq \|\psi_{\phi}^{0}\|_{G}^{2} \left(\frac{1}{1+\lambda \Delta t}\right)^{n+1} + \frac{R}{\lambda},$$

where  $\lambda = 2C_L^2 \alpha C_P^{-2}$ . Now the triangle inequality and G-norm equivalence complete the proof.  $\Box$ 

# 4. Numerical experiments

We now present results of three numerical tests that illustrate the theory above, and also show the importance of a careful choice of discretization. That is, while the AOT-DA theory at the PDE level is critical, in a discretization there are additional considerations and restrictions that can make the difference of a simulation succeeding or failing. All of our tests use Algorithm 3.1, i.e. the BDF2 IMEX-FEM algorithm studied above.

**Remark 4.1.** The theorems in previous sections give explicit bounds for the parameters  $\mu$ , H, etc. which guarantee convergence. However, these bounds only provide sufficient conditions for convergence, and it may be the case that

**Table 1** Velocity convergence rates of Algorithm 3.1 to the true solution with decreasing h and fixed  $\Delta t$  (left), fix h and decreasing  $\Delta t$  (middle), and also decreasing h and  $\Delta t$  at the same rate with  $\Delta t = 4h$  (right).

h	$\ v_h^n - u(t^n)\ $	Rate
1/4	4.12E-3	_
1/8	5.16E-4	3.00
1/16	5.91E-5	3.13
1/32	8.71E-6	2.76
1/64	1.92E-6	2.18
1/128	4.75E-7	2.02

$\Delta t$	$\ v_h^n - u(t^n)\ $	Rate
1	2.60E-3	1
1/2	3.63E-4	2.84
1/4	6.84E-5	2.41
1/8	1.52E-5	2.17
1/16	3.76E-6	2.02
1/32	1.09E-6	1.78

h	$\Delta t$	$\ v_h^n - u(t^n)\ $	Rate
1/4	1	4.69E-3	_
1/8	1/2	5.79E-4	3.02
1/16	1/4	9.16E-5	2.66
1/32	1/8	1.83E-5	2.32
1/64	1/16	4.38E-6	2.06
1/128	1/32	1.09E-6	2.00

convergence still happens when the bounds are not satisfied. It may very well be that the bounds are not sharp, or perhaps, even if the bounds are sharp, they take into account all possible initial conditions and parameters, including very extreme cases that may be unlikely to arise in typical simulations and experiments. Indeed, in practice, one finds that one has significantly more freedom to choose  $\mu$  and H in simulations than is suggested by the bounds. This phenomenon was first observed in [16], where convergence was observed when H – the largest distance between observation points – was chosen several orders of magnitude larger than the sufficient conditions given by the bounds. Therefore, in the computational experiments below, it is not surprising that convergence is seen even when the parameters do not satisfy the bound given above. Of course, the bounds are still useful, as they indicate certain scaling relations. Moreover, the existence of the bounds show that convergence is possible with finite positive parameters, implying that the algorithm is in principle possible to run on a finite machine. The experiments below show that, at least in the test cases we consider, it is also practical to do so.

# 4.1. Numerical Experiment 1: Convergence to an analytical solution

For our first experiment, we illustrate the convergence theory for Algorithm 3.1 for the chosen analytical solution on  $\Omega = (0, 1)^2$ .

$$u(x, y, t) = (\cos(y + t), \sin(x - t))^{T},$$
  
 $p(x, y, t) = \sin(2\pi(x + t)).$ 

We take  $\nu=0.01$ , and calculate the forcing function f using the continuous NSE,  $\nu$ , and the solution. Our computations use this time dependent f, nodally enforce Dirichlet boundary conditions on all sides to be equal to the true solution, and we use the initial conditions  $\nu_h^0=\nu_h^1=0$ . The operator  $I_H$  uses the same mesh used for velocity and pressure, and is defined to be the  $L^2$  projection onto piecewise constants on this mesh. This is known to satisfy our requirements for  $I_H$  in the theory (see e.g. Proposition 1.135 in [36]).

We first illustrate the theory with respect to convergence in h and  $\Delta t$ . For these calculations, we take  $\mu=10$ ,  $\gamma=1$ , and run to an end time of T=4.0 on a uniform mesh using Taylor–Hood elements. When observing the spatial convergence rates, we fix  $\Delta t=0.001$  and vary h, while for the temporal error we fix  $h=\frac{1}{64}$  and vary  $\Delta t$ . We also test spatial and temporal convergence together, by reducing h and  $\Delta t$ , but keeping the ratio  $4h=\Delta t$ . In all cases we observe second order convergence for spatial and temporal error, which is consistent with our analysis.

Table 1 displays the velocity convergence rates of Algorithm 3.1 solutions to the true solution; error is calculated using the  $L^2(\Omega)$  norm at the final time.

We also test convergence with respect to  $\mu$ . Our theory gives a sufficient condition for bounds on  $\mu$  that will guarantee convergence. To test this, we compute on a h=1/32 uniform mesh with Taylor–Hood elements and a time step size of  $\Delta t=0.01$ , up to T=5, and with varying  $\mu$ . Results are shown in Fig. 1 as the  $L^2(\Omega)$  difference between the AOT-DA computed solution and the true solution versus time. For clarity we show results for  $\mu \leq 10$  on the left and  $\mu \geq 10$  on the right. We observe that all choices of  $\mu$  provide convergence to the true solution, up to discretization error. Larger values of  $\mu$  converge faster, and convergence is monotonic until the level of discretization error is reached. It is interesting that convergence is achieved for all choices of  $\mu$ , no matter how large or small. This does not contradict our theory, which provides a sufficient condition on bounds for  $\mu$  that guarantee convergence; we conjecture for this problem that the use of time-dependent Dirichlet boundary condition enforcement and true forcing function f provide additional nudging of the AOT-DA solution towards the true solution, which may aid in convergence even when  $\mu$  is very small or very large.

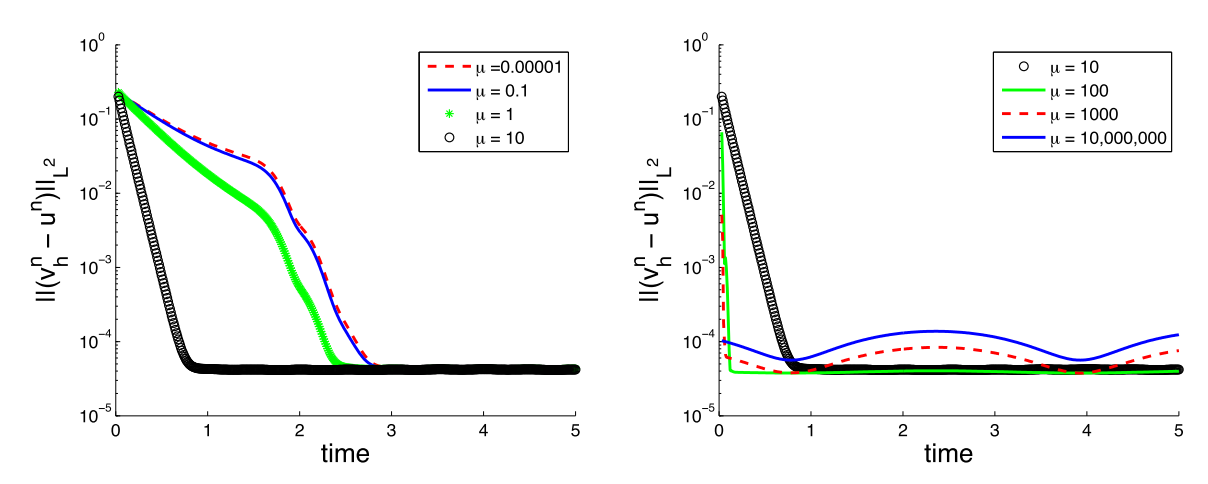


Fig. 1. Shown above are log-linear plots of convergence of the AOT-DA computed solutions to the true solution with increasing time t, for varying choices of the nudging parameter  $\mu$ . On the left is convergence for  $\mu < 10$ , and on the right is convergence for  $\mu > 10$ .

#### 4.2. Numerical Experiment 2: The no-flow test and pressure-robustness

For our second test, we show how the choice of finite elements can have a dramatic impact on the AOT-DA solution. The test problem we consider is the so-called 'no-flow test', where the forcing function of the NSE is given by  $Ra(0, y)^T$ , where Ra > 0 is a dimensionless constant (the Rayleigh number), and with Pr > 0 denoting the dimensionless Prandtl number:

$$\frac{1}{Pr}(u_t + u \cdot \nabla u) + \nabla p - \Delta u = Ra(0, y)^T, \tag{4.2}$$

$$\nabla \cdot u = 0, \tag{4.3}$$

$$u|_{\partial\Omega} = 0. (4.4)$$

This test problem corresponds to the physical situation of temperature driven flow (i.e. the Boussinesq system), with the temperature  $\theta$  profile specified to be stratified, i.e.  $f = Ra\theta e_2$  with  $\theta = y$ . Linear stratification is a natural steady state temperature profile. Since the forcing is potential, the solution to the system (4.2)–(4.4) with  $u_0 = 0$  initial condition is given by

$$u = 0, \ p = \frac{Ra}{2}y^2,$$

for any Pr > 0, hence the name no-flow.

We consider the no-flow test with Pr=1 and  $Ra=10^5$  (although this may seem like a large choice of a constant, for Boussinesq problems of practical interest, this choice of Ra is actually quite small). We use both Scott-Vogelius (SV) elements and Taylor-Hood (TH) elements, on a barycenter refined uniform discretization of the unit square with  $h=\frac{1}{32}$ . With TH elements, we use  $\gamma=0,1,10$ . We take  $I_H$  to be the  $X_h$  nodal interpolant (which satisfies the requirements of our theory since we are using  $X_h=P_2\cap X$ , see Theorem 1.103 in [36]). Since  $v_h^n\in X_h$  and  $u(t^n)=0\in X_h$ , the  $I_H$  operator acts simply as the identity operator. The time step size is chosen to be  $\Delta t=0.025$ , and solutions are computed up to end time T=0.8, using the  $X_h$  interpolant of  $(x\cos y, -\sin y)^T$  for  $v_h^0$ , and  $v_h^1$  is calculated from taking one step of the backward Euler AOT-DA scheme. The test is repeated for varying  $\mu$ .

Results of the simulations are displayed in Fig. 2, as  $L^2(\Omega)$  velocity error versus time. We observe a dramatic difference between SV and TH solutions. For  $\mu=1$  and  $\mu=10$ , all methods convergence, but the TH simulations only converge up to about  $10^{-3}$  while the SV simulations converge to  $10^{-9}$ . This is precisely due to error in the SV solution not depending on pressure (see Remark 3.11), which is large in this test problem. For  $\mu=0.1$ , the SV solution converges just as in the cases of larger  $\mu$ , but the TH solutions converge only up to  $10^{-1}$ , although it is unclear if this is simply failure to converge since this  $\mu$  is not large enough to satisfy the bounds on  $\mu$  in the theorem (in either case, SV gives a much better solution).

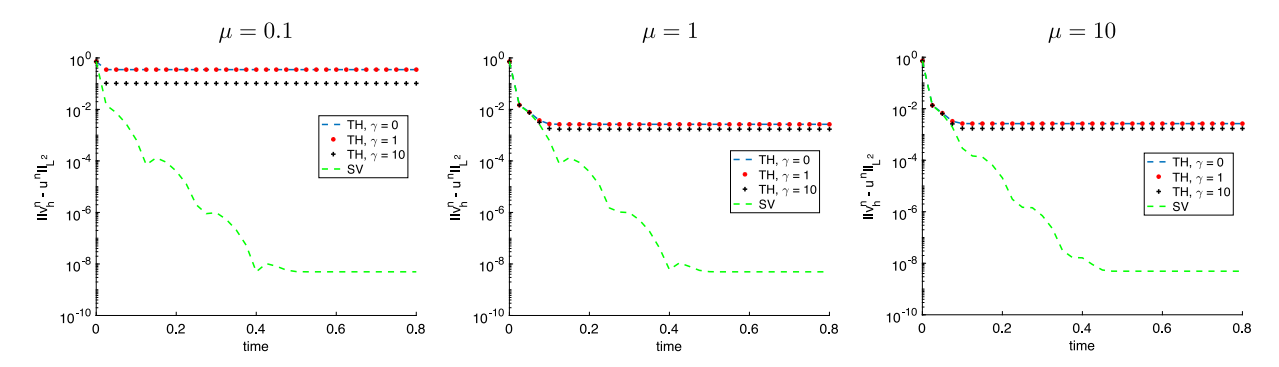


Fig. 2. Shown above is error in AOT-DA solutions for the no-flow solution, with SV element and TH elements (with varying  $\gamma$ ), with  $\mu = 0.1, 1.0, 10.0$  from left to right.

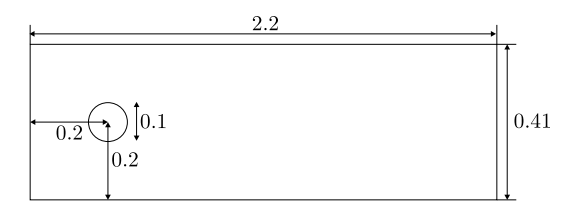


Fig. 3. Shown above is the domain for the flow past a cylinder test problem.

# 4.3. Numerical Experiment 3: 2D channel flow past a cylinder

For our last experiment, we consider Algorithm 3.1 applied to the common benchmark problem of 2D channel flow past a cylinder with Reynolds number 100 [44]. The domain is a  $2.2 \times 0.41$  rectangular channel with a cylinder of radius 0.05 centered at (0.2, 0.2), see Fig. 3. There is no external forcing, the kinematic viscosity is taken to be  $\nu = 0.001$ , no-slip boundary conditions are prescribed for the walls and the cylinder, while the inflow and outflow profiles are given by

$$u_1(0, y, t) = u_1(2.2, y, t) = \frac{6}{0.41^2}y(0.41 - y),$$
  
 $u_2(0, y, t) = u_2(2.2, y, t) = 0.$ 

Since we do not have access to a true solution for this problem, we instead use a computed solution. It is obtained using the same BDF2-IMEX-FEM scheme as in Algorithm 3.1 but without nudging (i.e.  $\mu = 0$ ), using  $(P_2, P_1^{disc})$  SV elements on a barycenter refined Delaunay mesh that provides 8658 elements and 60,994 total degrees of freedom, a time step of  $\Delta t = 0.002$ , and with the simulation starting from rest  $(u_h^0 = u_h^{-1} = 0)$ . We will refer to this solution as the DNS solution. Lift and drag calculations were performed for the computed solution and compared to the literature [44,45], which verified the accuracy of the DNS.

For the lift and drag calculations, we used the formulas

$$c_d(t) = 20 \int_{S} \left( v \frac{\partial u_{t_S}(t)}{\partial n} n_y - p(t) n_x \right) dS,$$
  
$$c_l(t) = 20 \int_{S} \left( v \frac{\partial u_{t_S}(t)}{\partial n} n_x - p(t) n_y \right) dS,$$

where p(t) is the pressure,  $u_{t_S}$  the tangential velocity S the cylinder, and  $n = \langle n_x, n_y \rangle$  the outward unit normal to the domain. For calculations, we use the global integral formula from [46].

For the AOT-DA algorithm, we start from  $v_h^1 = v_h^0 = 0$ , use the same spatial and temporal discretization parameters as the DNS, and start assimilation with the t = 5 DNS solution (i.e., time 0 for AOT-DA corresponds to t = 5 for

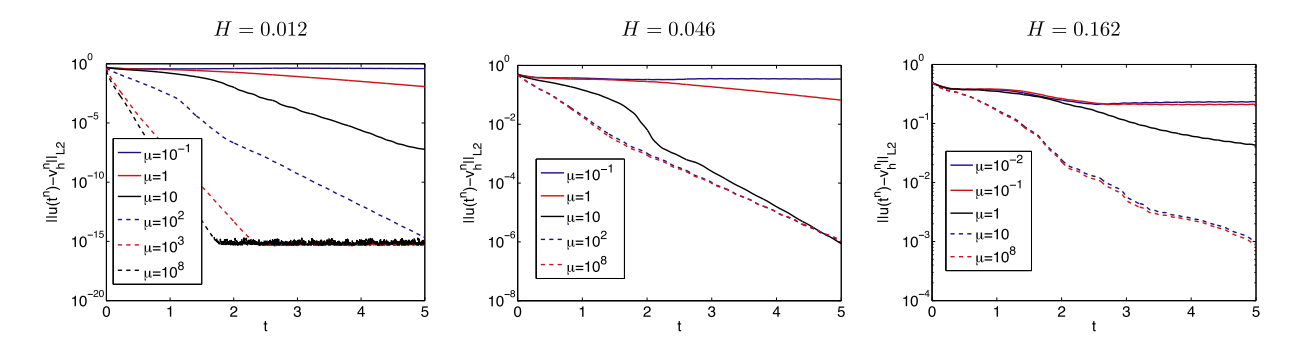


Fig. 4. Shown above is the  $L^2$  difference between the AOT-DA and DNS solutions versus time, for varying  $\mu$  and H.

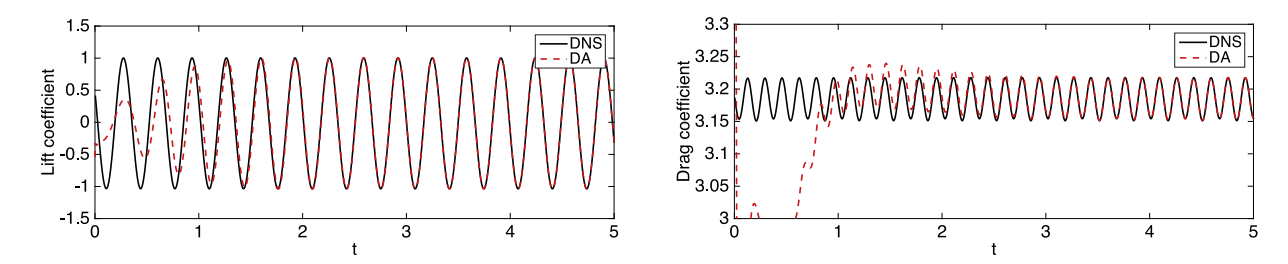


Fig. 5. Shown above is the difference between the AOT-DA ( $\mu = 10$  and H = 0.012) and DNS versus time, as difference in lift coefficients (top) and difference in drag coefficients (bottom).

the DNS). We define  $I_H$  to be the  $L^2$  projection onto constant functions on coarser meshes, and we compute with 3 different coarse meshes: the Delaunay mesh without the barycenter refinement which provided 2886 elements, and further coarsening to a 181 element mesh and a 15 element mesh. The average mesh width for these meshes is H = 0.012, 0.046, 0.162. The simulation is run on [0,5] (so the corresponding times for the DNS would be [5,10]), with varying  $\mu$  for each case of  $I_H$ .

Results are shown in Figs. 4–6. Fig. 4 shows the  $L^2$  error with time in each simulation. We observe that for each H, if  $\mu \le 1$  the AOT-DA solution does not sufficiently converge to the DNS solution by t=5, and does not show signs of converging in any time soon after. For  $\mu \ge 10$ , convergence of the AOT-DA solution to the DNS solution is observed for each H. However, we also observe the AOT-DA solution still converges to the DNS solution even for very large  $\mu$ , in fact there seems to be no negative impact on the convergence when taking  $\mu=10^8$  in the simulations. This does not contradict our theory, which guarantees convergence under the sufficient condition  $C(\text{data}, u) < \mu < \frac{2\nu}{C_I^2 h^2}$ , but does suggest an alternative convergence analysis may be possible for  $\mu$  outside this range.

Fig. 5 shows convergence of the lift and drag coefficients, for the simulation using H=0.012 and  $\mu=10$ . The lift coefficient converges fairly rapidly, with the AOT-DA and DNS plots matching closely by t=1.5. The drag coefficients are not in synch until about t=3. For this same simulation, we also show the convergence of the AOT-DA solution to the DNS solution in the speed contour plots in Fig. 6. Here, at t=0 there is a major difference, since the AOT-DA simulation starts from rest. The accuracy of AOT-DA is seen to increase by t=0.5 and further by t=1, and finally by t=2 there is only very slight differences observable between AOT-DA and DNS plots. By t=5, there is no visual difference between AOT-DA and DNS solutions.

# 5. Conclusions and future directions

We have analyzed and tested a BDF2 IMEX-FEM scheme for NSE with data assimilation. Under assumptions on the discretization parameters and regularity of the NSE solution, we proved long time stability and accuracy of the method. Moreover, the long time accuracy included exponential convergence in time of the AOT-DA solution to the true solution, up to discretization error. Several numerical tests were given to show the effectiveness of the scheme, and in particular we found that the element choice can make a dramatic difference in accuracy on certain problems.

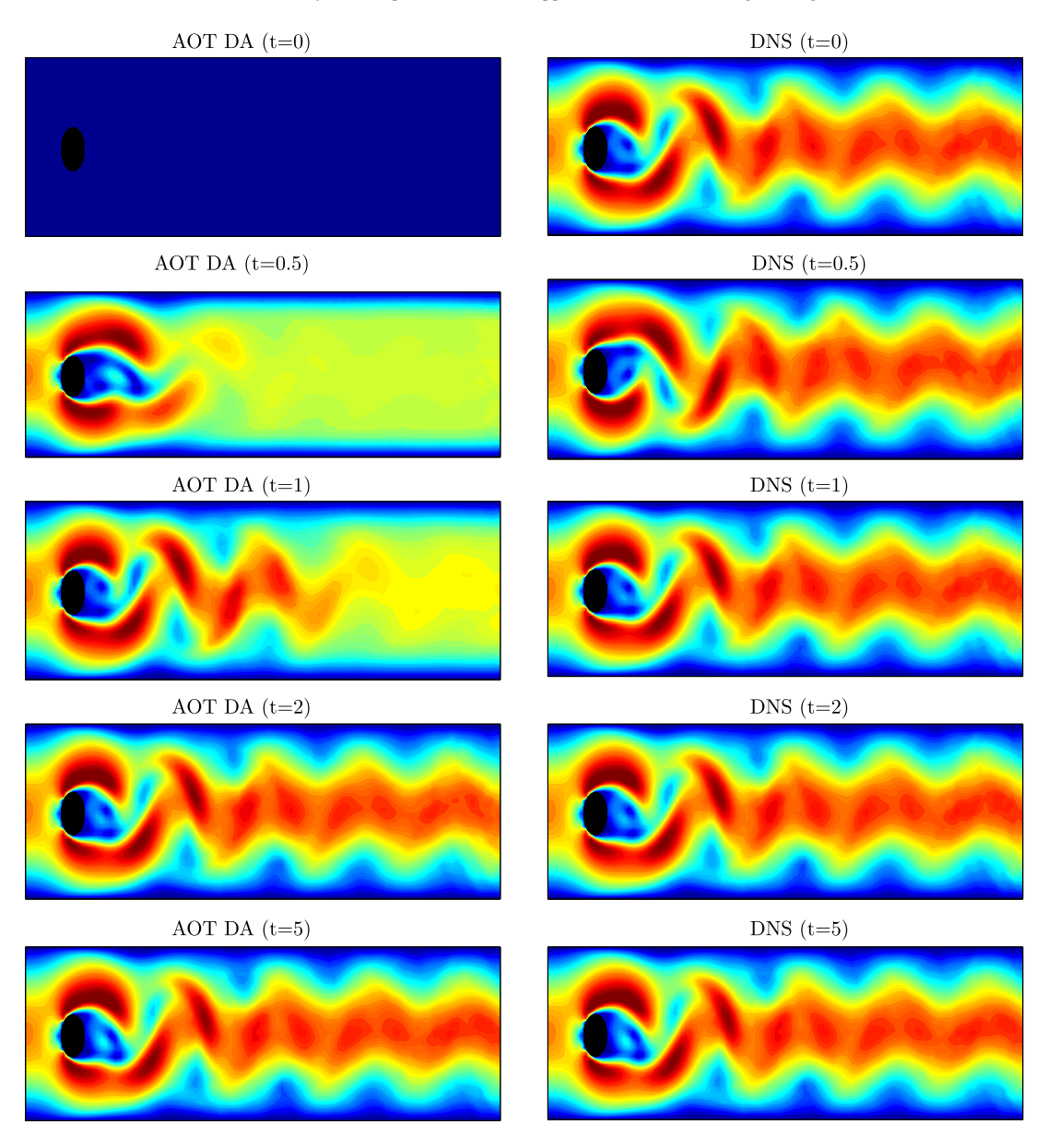


Fig. 6. Contour plots of AOT-DA and DNS velocity magnitudes at times 0, 0.5, 1, 2, and 5.

There are several future directions for research that arise from this work. First, our numerical tests showed the AOT-DA method tends to work for a much wider range of  $\mu$  than our theory requires. Thus there may be an improved analysis possible, in particular if one assumes a particular interpolation operator this might allow for an improved analysis. Other directions are to consider the AOT-DA approach for related coupled systems numerically, and also to consider long time accuracy in higher order norms.

# Acknowledgments

First author was partially supported by NSF Grant DMS 1716801. Second and third authors were partially supported by NSF Grant DMS 1522191.

#### References

- [1] R. Daley, Atmospheric Data Analysis, in: Cambridge Atmospheric and Space Science Series, Cambridge University Press, 1993.
- [2] E. Kalnay, Atmospheric Modeling, Data Assimilation and Predictability, Cambridge University Press, 2003.
- [3] K. Law, A. Stuart, K. Zygalakis, A Mathematical Introduction to Data Assimilation, in: Texts in Applied Mathematics, vol. 62, Springer, Cham, 2015, p. xviii+242.
- [4] J. Charney, M. Halem, R. Jastrow, Use of incomplete historical data to infer the present state of the atmosphere, J. Atmos. Sci. 26 (1969) 1160–1163.
- [5] A. Azouani, E. Olson, E.S. Titi, Continuous data assimilation using general interpolant observables, J. Nonlinear Sci. 24 (2) (2014) 277–304.
- [6] A. Azouani, E.S. Titi, Feedback control of nonlinear dissipative systems by finite determining parameters—a reaction-diffusion paradigm, Evol. Equ. Control Theory 3 (4) (2014) 579–594.
- [7] C. Cao, I.G. Kevrekidis, E.S. Titi, Numerical criterion for the stabilization of steady states of the Navier–Stokes equations, Indiana Univ. Math. J. 50 (Special Issue) (2001) 37–96. Dedicated to Professors Ciprian Foias and Roger Temam (Bloomington, IN, 2000).
- [8] K. Hayden, E. Olson, E.S. Titi, Discrete data assimilation in the Lorenz and 2D Navier-Stokes equations, Physica D 240 (18) (2011) 1416–1425.
- [9] E. Olson, E.S. Titi, Determining modes for continuous data assimilation in 2D turbulence, J. Stat. Phys. 113 (5–6) (2003) 799–840. Progress in statistical hydrodynamics (Santa Fe, NM, 2002).
- [10] D. Blömker, K. Law, A.M. Stuart, K.C. Zygalakis, Accuracy and stability of the continuous-time 3DVAR filter for the Navier-Stokes equation, Nonlinearity 26 (8) (2013) 2193–2219.
- [11] R.A. Anthes, Data assimilation and initialization of hurricane prediction models, J. Atmos. Sci. 31 (3) (1974) 702–719.
- [12] J.E. Hoke, R.A. Anthes, The initialization of numerical models by a dynamic-initialization technique, Mon. Weather Rev. 104 (12) (1976) 1551–1556.
- [13] S. Lakshmivarahan, J.M. Lewis, Nudging methods: A critical overview, in: Data Assimilation for Atmospheric, Oceanic and Hydrologic Applications (Vol. II), Springer, 2013, pp. 27–57.
- [14] H. Bessaih, E. Olson, E.S. Titi, Continuous data assimilation with stochastically noisy data, Nonlinearity 28 (3) (2015) 729–753.
- [15] C. Foias, C.F. Mondaini, E.S. Titi, A discrete data assimilation scheme for the solutions of the two-dimensional Navier-Stokes equations and their statistics, SIAM J. Appl. Dyn. Syst. 15 (4) (2016) 2109–2142.
- [16] M. Gesho, E. Olson, E.S. Titi, A computational study of a data assimilation algorithm for the two-dimensional Navier-Stokes equations, Commun. Comput. Phys. 19 (4) (2016) 1094–1110.
- [17] M.U. Altaf, E.S. Titi, O.M. Knio, L. Zhao, M.F. McCabe, I. Hoteit, Downscaling the 2D Benard Convection Equations Using continuous data assimilation, Comput. Geosci. 21 (3) (2017) 393–410.
- [18] A. Larios, Y. Pei, Nonlinear continuous data assimilation, submitted for publication, arXiv:1703.03546.
- [19] E. Lunasin, E.S. Titi, Finite determining parameters feedback control for distributed nonlinear dissipative systems—a computational study, Evol. Equ. Control Theory 6 (4) (2017) 535–557.
- [20] D.A. Albanez, H.J. Nussenzveig Lopes, E.S. Titi, Continuous data assimilation for the three-dimensional Navier–Stokes-α model, Asymptot. Anal. 97 (1–2) (2016) 139–164.
- [21] A. Biswas, V.R. Martinez, Higher-order synchronization for a data assimilation algorithm for the 2D Navier–Stokes equations, Nonlinear Anal. RWA 35 (2017) 132–157.
- [22] A. Farhat, M.S. Jolly, E.S. Titi, Continuous data assimilation for the 2D Bénard convection through velocity measurements alone, Physica D 303 (2015) 59–66.
- [23] A. Farhat, E. Lunasin, E.S. Titi, Abridged continuous data assimilation for the 2D Navier–Stokes equations utilizing measurements of only one component of the velocity field, J. Math. Fluid Mech. 18 (1) (2016) 1–23.
- [24] A. Farhat, E. Lunasin, E.S. Titi, Data assimilation algorithm for 3D Bénard convection in porous media employing only temperature measurements, J. Math. Anal. Appl. 438 (1) (2016) 492–506.
- [25] A. Farhat, E. Lunasin, E.S. Titi, On the Charney conjecture of data assimilation employing temperature measurements alone: the paradigm of 3D planetary geostrophic model, Math. Clim. Weather Forecast. 2 (1) (2016).
- [26] A. Farhat, E. Lunasin, E.S. Titi, Continuous data assimilation for a 2D Bénard convection system through horizontal velocity measurements alone, J. Nonlinear Sci. (2017) 1–23.
- [27] K. Foyash, M.S. Dzholli, R. Kravchenko, È.S. Titi, A unified approach to the construction of defining forms for a two-dimensional system of Navier-Stokes equations: the case of general interpolating operators, Uspekhi Mat. Nauk 69 (2(416)) (2014) 177–200.
- [28] N. Glatt-Holtz, I. Kukavica, V. Vicol, M. Ziane, Existence and regularity of invariant measures for the three dimensional stochastic primitive equations, J. Math. Phys. 55 (5) (2014) 051504, 34.
- [29] M.S. Jolly, V.R. Martinez, E.S. Titi, A data assimilation algorithm for the subcritical surface quasi-geostrophic equation, Adv. Nonlinear Stud. 17 (1) (2017) 167–192.
- [30] M.S. Jolly, T. Sadigov, E.S. Titi, A determining form for the damped driven nonlinear Schrödinger equation—Fourier modes case, J. Differential Equations 258 (8) (2015) 2711–2744.
- [31] A. Larios, E. Lunasin, E.S. Titi, Global well-posedness for the Boussinesq-Voigt equations, (preprint) arXiv:1010.5024.
- [32] P.A. Markowich, E.S. Titi, S. Trabelsi, Continuous data assimilation for the three-dimensional Brinkman–Forchheimer-extended Darcy model, Nonlinearity 29 (4) (2016) 1292.
- [33] C.F. Mondaini, E.S. Titi, Uniform-in-time error estimates for the postprocessing Galerkin method applied to a data assimilation algorithm, SIAM J. Numer. Anal. 56 (1) (2018) 78–110.

- [34] H. Ibdah, C. Mondaini, E. Titi, Space-time discrete numerical schemes for a feedback-control data assimilation algorithm, in preparation, 2018.
- [35] E. Olson, E.S. Titi, Determining modes and Grashof number in 2D turbulence: a numerical case study, Theor. Comput. Fluid Dyn. 22 (5) (2008) 327–339.
- [36] A. Ern, J.-L. Guermond, Theory and Practice of Finite Elements, Vol. 159, Springer Science & Business Media, 2013.
- [37] E. Hairer, G. Wanner, Solving Ordinary Differential II: Stiff and Differential-Algebraic Problems, second ed., Springer, 2002.
- [38] W. Chen, M. Gunzburger, D. Sun, X. Wang, Efficient and long-time accurate second-order methods for Stokes-Darcy system, SIAM J. Numer. Anal. 51 (2013) 2563–2584.
- [39] V. John, A. Linke, C. Merdon, M. Neilan, L.G. Rebholz, On the divergence constraint in mixed finite element methods for incompressible flows, SIAM Rev. 59 (3) (2017) 492–544.
- [40] V. Girault, P.-A. Raviart, Finite Element Methods for Navier-Stokes Equations: Theory and Algorithms, Springer-Verlag, 1986.
- [41] W. Layton, Introduction to Finite Element Methods for Incompressible, Viscous Flow, SIAM, Philadelphia, 2008.
- [42] R. Temam, Navier-Stokes Equations: Theory and Numerical Analysis, North Holland Publishing Company, New York, 1977.
- [43] S. Brenner, L. Scott, The Mathematical Theory of Finite Element Methods, 3rd edition, Springer-Verlag, 2008.
- [44] M. Schäfer, S. Turek, The benchmark problem 'flow around a cylinder' flow simulation with high performance computer II., Notes Numer. Fluid Mech. 52 (1996) 547–566.
- [45] M. Mohebujjaman, L. Rebholz, X. Xie, T. Iliescu, Energy balance and mass conservation in reduced order models of fluid flows, J. Comput. Phys. 346 (2017) 262–277.
- [46] V. John, Reference values for drag and lift of a two dimensional time-dependent flow around a cylinder, Internat. J. Numer. Methods Fluids 44 (2002) 777–788.